mater.scichina.com link.springer.com

Published online 17 February 2023 | https://doi.org/10.1007/s40843-022-2344-2
Sci China Mater 2023, 66(5): 1801–1809

Synergistic Cu^+/Cu^0 on Cu_2O-Cu interfaces for efficient and selective C_{2+} production in electrocatalytic CO_2 conversion

Shengnan Wang[1,2†], Dan Wang[1†], Benqiang Tian[2†], Xiangxiang Gao[2†], Lu Han[2], Yang Zhong[3], Shuchang Song[2], Zhili Wang[2], Yaping Li[2], Jianing Gui[1], Marshet G. Sendeku[4], Ying Zhang[1*], Yun Kuang[2*] and Xiaoming Sun[2]

ABSTRACT **The electrocatalytic CO_2 reduction technology is expected to simultaneously alleviate increasing CO_2 emissions and the depletion of fossil resources. However, it is still a big challenge to improve the selectivity toward valuable multi-carbon products in electrocatalytic CO_2 reduction reaction. In this study, the synergistic role of Cu^+ and Cu^0 species in Cu_2O-Cu interfaces is unravelled through density functional theory (DFT) calculations, in which the electrode surface exhibits low free energy of *COCO intermediate formation and H_2O dissociation, which are beneficial to the high selectivity towards multi-carbon products, especially C_2H_4. Guided by these DFT results, an oxide-derived copper electrode activation strategy that builds the synergistic Cu^+ and Cu^0 on Cu_2O-Cu interfaces is designed to boost the selectivity toward multi-carbon products. Interestingly, Cu_2O cubes chosen as the pristine catalyst are activated *via* a square-wave (SW) potential treatment to form SW-Cu_2O cubes that bear Cu^+ and Cu^0 species. The as-prepared SW-Cu_2O cubes exhibit superior Faradaic efficiencies for C_2H_4 (60%) and C_{2+} products (75%) in an H-type cell, which are about 1.5 times that of the Cu_2O cubes. This study demonstrates the synergistic Cu^0 and Cu^+ on Cu_2O-Cu interfaces for improving the selectivity of a specific valuable multi-carbon product in electrocatalytic CO_2 conversion.**

Keywords: Cu^+ and Cu^0, C–C coupling, CO_2RR, Cu_2O-Cu interfaces, square-wave

INTRODUCTION

Converting CO_2 into fuels and value-added chemicals is a promising route to alleviate increasing CO_2 emissions and achieve a sustainable carbon-neutral energy conversion in industrial society [1–3]. Particularly, CO_2 electroreduction technology utilizing renewable electricity can effectively store energy in the form of chemical bonds by breaking and rearranging the strong bonding in CO_2 and water, thereby generating fuels and valuable chemicals [4,5]. Until recently, the electrocatalytic CO_2 reduction reaction (ECO_2RR) to form C_1 products (CO and HCOOH) has been achieved with a high Faradaic efficiency (FE > 90%) and partial current density almost close to the industrial level [6–9]. However, the production of multi-carbon valuable compounds from ECO_2RR still remains a challenge due to the difficulty in restraining the kinetically favored hydrogen evolution reaction (HER) and the low selectivity toward specific products. Therefore, designing electrodes with high activity and selectivity toward multi-carbon products for ECO_2RR remains one of the major priorities [10]. Among various electrocatalysts reported for ECO_2RR, metallic Cu and Cu-based materials have shown great potential to produce multi-carbon products in aqueous solutions due to their suitable adsorption energy for the key intermediate (*CO) during CO_2 transformation [11–13]. Nevertheless, these electrocatalysts suffer from moderate binding energies with most intermediates (i.e., *CHO, *COCO, or *COCOH), which leads to low selectivity toward valuable product formation [14–16].

Previous studies reported that Cu^{2+} species are not active sites in ECO_2RR [14,17]. Intriguingly, an electrode surface with a dominant low chemical state of Cu (oxidized Cu^+ and metallic Cu^0) has been reported to offer higher yields of valuable products (i.e., C_2H_4, C_2H_5OH, CO, CH_4, and HCOOH) [17]. Moreover, the importance of Cu^+ species towards CO_2 transformation was confirmed by electrocatalytic selectivity studies on ECO_2RR. For instance, Cuenya's group [18] demonstrated the oxidized Cu (Cu^+) surface can produce C_2H_4 with higher selectivity compared with the H_2-plasma treated Cu surface (Cu^0). Following this seminal study, the presence of Cu^+ species was speculated to alter the thermodynamic adsorption energies of the key intermediates as well as the kinetic barrier of the reaction, which led to the change in ECO_2RR pathways [19]. Additionally, Lee's group [20] reported that the mixed Cu^+ and Cu^0 states favored C_{2+} production, in which the Cu_2O layer with mixed Cu^+ and Cu^0 states exhibited enhanced selectivity toward C_2H_4. Some other reports also revealed that the Cu electrode with different degrees of oxidation state (mixed Cu^+ and Cu^0) is

[1] Key Laboratory of Synthetic and Biological Colloids, Ministry of Education, School of Chemical and Material Engineering, Jiangnan University, Wuxi 214122, China
[2] State Key Laboratory of Chemical Resource Engineering, Beijing Advanced Innovation Center for Soft Matter Science and Engineering, College of Chemistry, Beijing University of Chemical Technology, Beijing 100029, China
[3] Weichai Power Co., Ltd., Weifang 261061, China
[4] Ocean Hydrogen Energy R&D Center, Research Institute of Tsinghua University in Shenzhen, Shenzhen 518000, China
† These authors contributed equally to this work.
* Corresponding authors (emails: kuangyun@mail.buct.edu.cn (Kuang Y); ying.zhang@jiangnan.edu.cn (Zhang Y))

capable of directing a particular CO_2RR pathway to obtain the corresponding C_2H_4/C_2H_5OH products [21,22]. To further investigate the positive effects of Cu^+ and Cu^0 on efficient and selective C_{2+} production, the roles of Cu^+ and Cu^0 for CO_2 adsorption and activation as well as H_2O dissociation for boosting the C–C coupling and improving multi-carbon production are discussed using theoretical analysis in this work. Density functional theory (DFT) calculations reveal that the synergistic Cu^+ and Cu^0 on Cu_2O-Cu interfaces facilitate the formation of *COCO intermediates with low free energy and H_2O dissociation on the electrode surface, which is beneficial to the high selectivity towards multi-carbon production, especially C_2H_4 formation.

Inspired by the DFT findings, an oxide-derived copper electrode activation strategy that builds the synergistic Cu^+ and Cu^0 sites on Cu_2O-Cu interfaces was designed. The pristine Cu_2O cubes were activated *via* a square-wave (SW) potential treatment to form SW-Cu_2O cubes. Interestingly, the fast and periodic exposure to anodic and cathodic potentials in the process of SW significantly modified the distribution of Cu species on the surface of Cu_2O cubes and formed SW-Cu_2O cubes with uniformly distributed Cu^+/Cu^0 interfaces. The designed structure exhibits high FEs for C_2H_4 (~60%) and C_{2+} products (~75%), which is about 1.5 times higher than that of pristine Cu_2O cubes (~39% for C_2H_4 and ~51% for C_{2+} products) under optimal conditions. Moreover, the as-prepared SW-Cu_2O/Cu cubes also display a higher partial current density for C_2H_4 (~60 mA cm^{-2}) in an H-type cell, which is about 2.3 times higher than that of pristine Cu_2O cubes. Therefore, SW-Cu_2O cubes can be regarded as a model catalyst for C_{2+} production, due to the synergistic effect of Cu^+ and Cu^0 on Cu_2O-Cu interfaces, which improves the key processes of C–C coupling and H_2O dissociation in ECO_2RR. Furthermore, creating effective interfaces with Cu^0 and Cu^+ species can also be extended to design other Cu metal and Cu-based catalytic systems to boost the selectivity of electrodes toward a specific valuable multi-carbon product.

EXPERIMENTAL SECTION

Synthesis of pristine Cu_2O cubes

Cu_2O cubes were synthesized *via* a wet chemical reduction method according to a previous report [23]. Firstly, 2.0 mL of 0.9 mol L^{-1} $C_6H_5Na_3O_7{\cdot}2H_2O$ was added into 400 mL of distilled water and stirred for 20 min. Then 2.0 mL of 1.2 mol L^{-1} $CuSO_4{\cdot}5H_2O$ aqueous solution was rapidly added into the above solution and stirred for 5 min. Next, 2.0 mL of 4.8 mol L^{-1} NaOH aqueous solution was added to the above-mixed solution and contineously stirred for 5 min to obtain a blue solution. Finally, 2.0 mL of 1.2 mol L^{-1} ascorbic acid solution was added into the obtained blue solution and stirred for 30 min to obtain the orange-yellow turbid liquid. The obtained precipitate was collected by centrifugation and then washed with distilled water and methanol. Afterward, the as-prepared orange powder was dried under a vacuum at 60°C for 6 h.

Cu_2O cubes activated by SW

A certain amount of pristine Cu_2O cubes was loaded onto a gas diffusion layer electrode. The pristine Cu_2O was activated *via* SW in a CO_2-saturated 0.1 mol L^{-1} $KHCO_3$ electrolyte by alternating the oxidation and reduction potentials and SW treatment was also employed for different times to obtain SW-Cu_2O/Cu electrodes at a fixed pulse time of 0.1 s.

Theoretical calculations

In the present work, the geometric structures of models were first optimized to obtain the corresponding energy values, and then electronic structures and other properties were calculated under the optimized geometric structure. The calculations were performed to obtain structural parameters and electronic properties by using Vienna *ab-initio* Simulation Package (VASP) in the framework of DFT [24,25]. The ion-electron interaction was described by the projector-augmented wave (PAW) method [26]. The exchange-correlation potential was treated using the generalized gradient approximation (GGA) parameterized by Perdew-Burke-Ernzerhof (PBE) approach [27]. Each atom in the reactant and product was relaxed by the conjugate gradient method. The plane wave cut-off energy was 450 eV and the Brillouin Zone (BZ) integral was automatically generated by the Monkhorst-Pack method (5 × 5 × 1) irreducible *k*-space grid. The bulk spin was not restricted and the internal stress convergence standard of the crystal was 0.02 GPa. The single-atom energy convergence standard was $<10^{-4}$ eV $Å^{-1}$, and the convergence standard of the interaction force between atoms was 0.01 eV nm^{-1}. The calculation model of Cu_2O and Cu_2O-Cu included six layers and the unit cell was separated by a vacuum layer with a thickness greater than 15 Å in the *Z*-axis direction to avoid electrostatic Coulomb interaction between atoms on the upper and lower surfaces. The three layers of atoms below were fixed while relaxing other atoms at the same time.

RESULTS AND DISCUSSION

DFT calculations

Previous experimental efforts have unveiled the role of Cu^+ and Cu^0 species on ECO_2RR products. To investigate their synergistic influence and further uncover the mechanism for the enhanced selectivity toward C_{2+} production, a theoretic analysis was conducted. The Cu_2O-Cu model is used to simulate the Cu^+/Cu^0 interfaces, in which some Cu^0 crystalline domains are embedded in the Cu_2O crystal. The crystal structure models of Cu_2O (100) and Cu_2O-Cu (100) are shown in Fig. 1a, b. The electronic analysis of Cu_2O and Cu_2O-Cu was performed by density of states (DOS), as shown in Fig. S1. It can be seen that the energy bandgap of Cu_2O-Cu (0.78 eV) is lower than that of Cu_2O (1.25 eV), illustrating the enhanced conductivity of Cu_2O-Cu. Additionally, the electronic structures of Cu_2O and Cu_2O-Cu were first studied *via* DFT calculations to explore the relationship between the structure and their ECO_2RR performance. From the local charge on Cu_2O and Cu_2O-Cu (Fig. 1c, d), the arrangement of the electrons between Cu^+ ions in Cu_2O crystal is relatively concentrated and isolated. Whereas, the electron distribution on Cu^+ ions and Cu^0 atoms of Cu_2O-Cu is in a connected form, thus improving the conductivity and facilitating the progress of surface catalytic reactions. Furthermore, the charge difference for the adsorption of CO_2 molecules on the surface of Cu_2O and Cu_2O-Cu is shown in Fig. S2. The adsorption of CO_2 molecules on the surface of Cu_2O in Fig. S2a shows that the electrons are mainly concentrated between Cu^+ ions in Cu_2O crystals and C atoms in CO_2 molecules, which indicates the vertical adsorption configuration. While influenced by the arrangement of the electrons between Cu^+ ions and Cu^0 atoms on Cu_2O-Cu, the adsorption of CO_2 molecules on Cu_2O-Cu

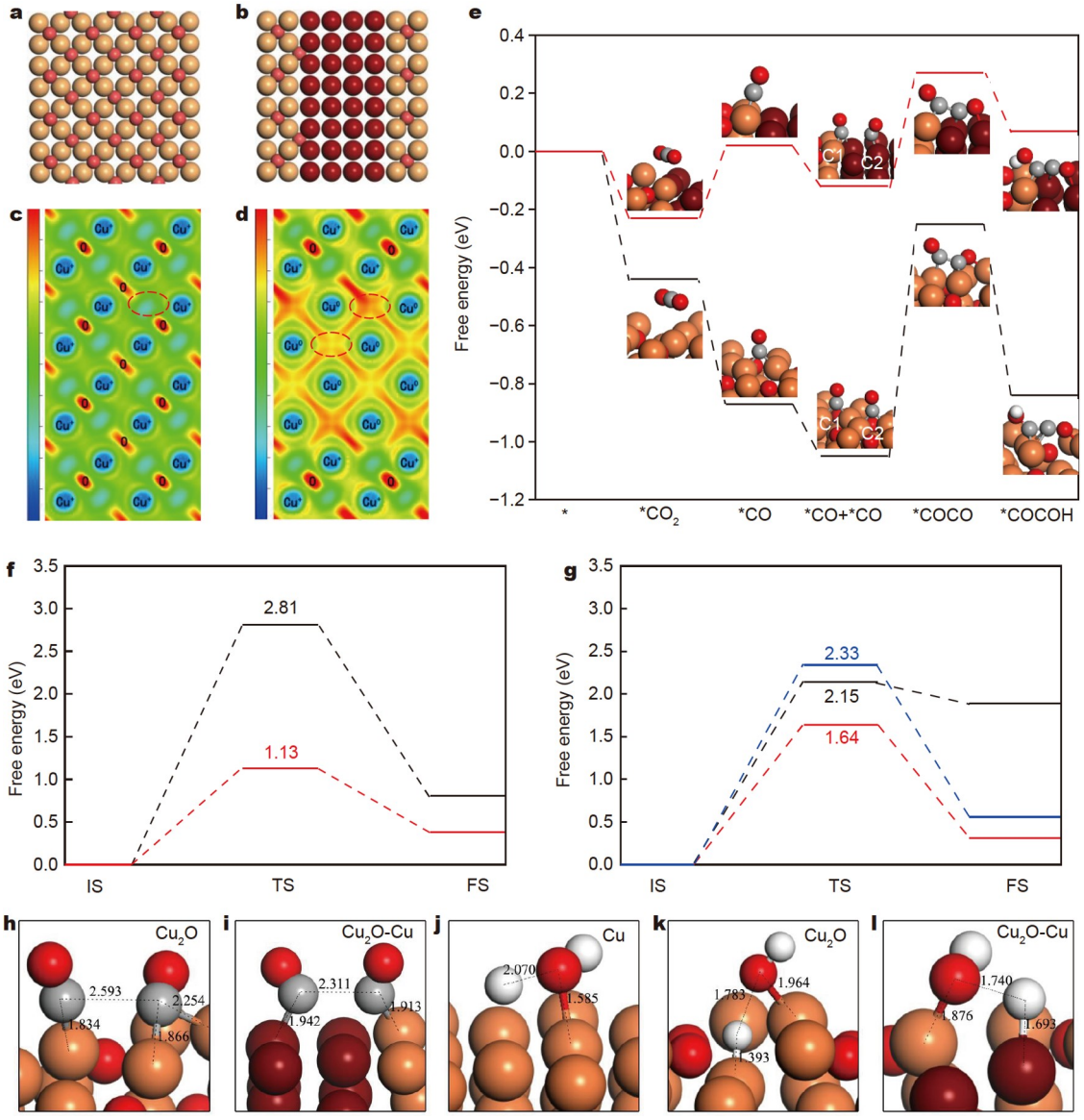

Figure 1 Theoretical calculations on Cu_2O and Cu_2O-Cu interfaces. The top view of the structure model of (a) Cu_2O (100) and (b) Cu_2O-Cu (100). Local-charge of (c) Cu_2O (100) and (d) Cu_2O-Cu (100). (e) Free energy profiles of CO_2RR on Cu_2O (100) (black line) and Cu_2O-Cu (100) (red line). (f) Energy barriers of *CO dimerization (*CO + *CO → *COCO) on Cu_2O (100) (black line) and Cu_2O-Cu (100) (red line). (g) Energy barriers of H_2O dissociation (*H_2O → *H + *OH) on Cu (100) (blue line), Cu_2O (100) (black line), and Cu_2O-Cu (100) (red line). Optimized structure of *CO dimerization on the surface of (h) Cu_2O and (i) Cu_2O-Cu. Optimized structure of H_2O dissociation on the surface of (j) Cu, (k) Cu_2O, and (l) Cu_2O-Cu. The dark red, dark orange, red, grey, and white spheres represent Cu^0, Cu^+, O, C, and H, respectively.

(Fig. S2b) exhibits that the electrons are mainly concentrated between the CO groups in CO_2 molecules and Cu^0 atoms on Cu_2O-Cu and the electrons are more inclined to the side of CO. This indicates that the crucial *CO intermediates in ECO_2RR are much easier to form on Cu_2O-Cu interfaces. In addition, the electron density on C atoms in the *CO intermediate on the surface of Cu_2O and Cu_2O-Cu was analyzed by the Bader charge analysis, as shown in Fig. S3. The electron density around the C atoms in *CO intermediates on Cu_2O-Cu is significantly increased compared with that on Cu_2O, suggesting the presence of more electrons on the adjacent C atoms in *CO intermediates for coupling reactions to form *CO dimerization [28].

To further explore the influence of the electronic structure distinction between Cu_2O and Cu_2O-Cu on ECO_2RR towards C_2H_4, the possible ECO_2RR pathway was investigated by DFT using Cu_2O (100) and Cu_2O-Cu (100) models [29–31]. The *CO dimerization is regarded as a critical step toward C_{2+} product formation [16,32]. The free energy profiles of forming *CO and its dimerization to form *COCO are presented in Fig. 1e. As noted, the potential barrier of *CO dimerization on Cu_2O (100) is higher than that on Cu_2O-Cu (100), which indicates the ease of *CO dimerization on Cu_2O-Cu than on Cu_2O. To verify that *CO dimerization tends to form on Cu_2O-Cu, the reaction energy barrier and transition state of *CO dimerization on Cu_2O (100) and Cu_2O-Cu (100) were simulated (Fig. 1f), and the corresponding optimized structure of *CO dimerization on the surface of Cu_2O and Cu_2O-Cu are shown in Fig. 1h, i and Fig. S4. The bond length of C–C and the energy barrier of *CO dimerization on Cu_2O-Cu (100) are about 2.311 Å and 1.13 eV, while it is about 2.593 Å and 2.81 eV on Cu_2O (100). The shorter

bond length between C–C and the lower *CO dimerization energy barrier on Cu_2O-Cu further confirm that *CO dimerization on Cu_2O-Cu is more easily than that on Cu_2O. Furthermore, H^+ ions dissociated from H_2O also play an important role in ECO_2RR for multi-carbon products. Therefore, it is very important to explore the energy barriers of H_2O dissociation on Cu, Cu_2O, and Cu_2O-Cu [33–35]. Fig. 1g exhibits the energy barriers of H_2O dissociation on Cu, Cu_2O, and Cu_2O-Cu and the corresponding optimized structures are shown in Fig. 1j–l and Fig. S5. The energy barrier of H_2O dissociation on the surfaces of Cu, Cu_2O, and Cu_2O-Cu is about 2.33, 2.15, and 1.64 eV, respectively. Therefore, the H_2O dissociation is easier to occur on the surface of Cu_2O-Cu interfaces, which can provide more H^+ for C_{2+} products. Based on the above analysis, Cu_2O-Cu can be designed as a model catalyst for ECO_2RR to C_{2+} products, especially C_2H_4. The synergistic Cu^+ and Cu^0 on Cu_2O-Cu interfaces could facilitate *COCO intermediate formation and H_2O dissociation [29].

Catalyst synthesis and characterization

Our DFT calculation shows that Cu^+ and Cu^0 on Cu_2O-Cu interfaces could play a synergistic role in obtaining the CO dimerization toward C_{2+} product formation. Based on this analysis, a facile SW method was utilized to rationally design Cu_2O-Cu interfaces with uniformly distributed Cu^+/Cu^0 (Fig. 2a). Firstly, Cu_2O was synthesized by a wet chemical reduction method [23]. Then the as-prepared Cu_2O was activated *via* SW with alternating oxidation and reduction potentials five times a second and maintained for 30 min in a CO_2-saturated 0.1 mol L^{-1} $KHCO_3$ electrolyte to form Cu_2O-Cu interfaces (denoted as SW-Cu_2O). The oxidation and reduction potentials applied to obtain SW-Cu_2O were 0.8 and −0.4 V (all potentials hereafter were given with respect to reversible hydrogen electrode (RHE)), respectively. The applied SW potentials were chosen according to the cyclic voltammetry (CV) curve of Cu_2O in Fig. S6. The selected oxidation potential is slightly more positive than the oxidation potential of Cu to Cu_2O and the reduction potential is more negative than the reduction potential of Cu_2O to Cu. In the course of SW, the redox shuttle manner by the periodical cycling between oxidation and reduction processes was utilized to obtain uniformly distributed Cu^+ and Cu^0 species on the surface of Cu_2O.

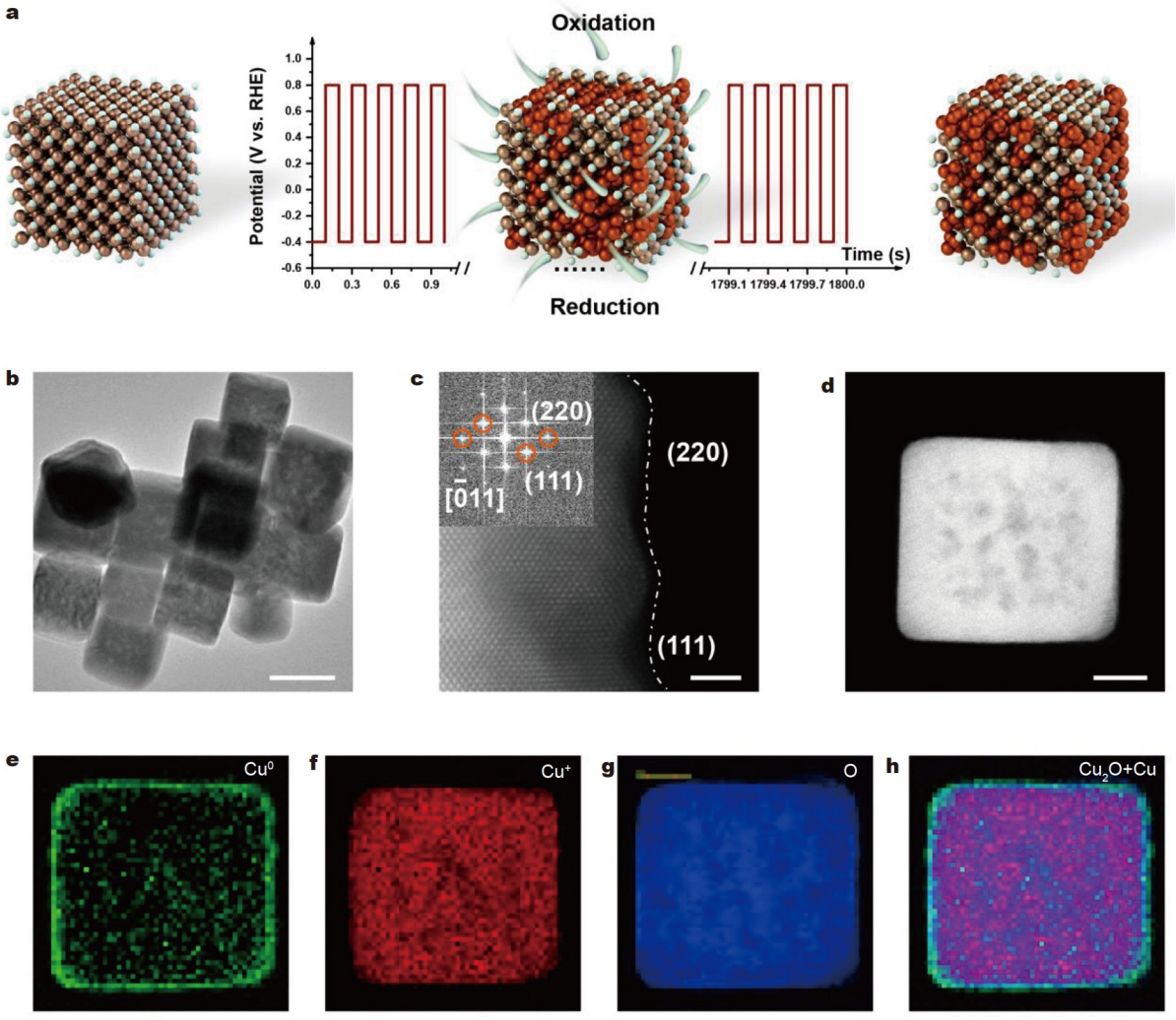

Figure 2 Preparation and characterization of SW-Cu_2O cubes. (a) Schematic illustration of the fabrication procedure of SW-Cu_2O/Cu cubes. The red, champagne and cyan spheres represent Cu^0, Cu^+ and O, respectively. (b) HRTEM image of SW-Cu_2O/Cu cubes (scale bar: 100 nm). (c) HRSTEM bright-field image of an SW-Cu_2O cube (scale bar: 2 nm) and the corresponding FFT pattern (in the top left). (d) STEM image of a single SW-Cu_2O cube (scale bar: 20 nm). (e–h) High magnification elemental mapping of Cu^0, Cu^+, and O by the STEM-EELS spectrum imaging (scale bar: 20 nm).

Microscopic characterizations were conducted to reveal the morphology features of the pristine Cu_2O and as-prepared SW-Cu_2O. The transmission electron microscopy (TEM) image in Fig. S7a shows that the morphology of the pristine Cu_2O is a cubic shape with a size of about 100 nm. The high-resolution TEM (HRTEM) image of a pristine Cu_2O cube in Fig. S7b reveals the obvious lattice fringes of 0.212 nm, corresponding to the (200) planes of Cu_2O. The TEM image of the as-prepared SW-Cu_2O (Fig. 2b) indicates that the cubic shape of Cu_2O is retained during the SW process. The high-resolution scanning TEM (HRSTEM) bright-field image of an SW-Cu_2O cube in Fig. 2c shows the concave-convex structure with different orientations on the edges, corresponding to (220) and (111) planes of Cu_2O. The fast Fourier transform (FFT) pattern of the SW-Cu_2O cube (inset of Fig. 2c) is also indexed to the (220) and (111) planes of Cu_2O. The different orientation planes between SW-Cu_2O (Fig. 2c) and pristine Cu_2O cubes (Fig. S7b) could be attributed to the reconstruction of the Cu_2O surface during the SW process. Furthermore, the STEM image of the as-synthesized SW-Cu_2O cube (Fig. 2d) and the atomic-scale electron energy-loss spectroscopy (EELS) profiles across an SW-Cu_2O cube (Fig. 2e–g) were investigated to identify their elemental distributions. It can be seen that Cu^0 and Cu^+ species coexist but distribute in different positions of the SW-Cu_2O cubes. The Cu^+ species distribute throughout the cube corresponding exactly to the O distribution, while Cu^0 mainly distributes on the surface of the SW-Cu_2O cubes, which contrasts sharply with the elemental distribution of the pristine Cu_2O nanocube (Fig. S8). The mixed elemental mapping image in Fig. 2h further demonstrates that Cu^+ and Cu^0 species coexist on the surface of the SW-Cu_2O cubes.

The X-ray diffraction (XRD) technique was employed to investigate the phase structure of Cu_2O before and after SW. As shown in Fig. 3a, the main phase of pristine Cu_2O (JCPDS: 34-1354) is retained after SW for 30 min. The peaks indexed to Cu (111) and Cu(200) (JCPDS: 04-0836) are remained after being activated *via* SW for 30 min, demonstrating the coexistence of metallic Cu and Cu_2O in SW-Cu_2O. Additionally, the extra peaks appearing in the XRD diffractogram belong to the substrate. Furthermore, the XRD patterns of fresh Cu_2O and after different times of SW activation are shown in Fig. S9. The relative intensity of (111) and (200) peaks of metallic Cu becomes higher with prolonging the SW time from 15 to 60 min, which indicates that the composition of Cu_2O-Cu interfaces could be adjusted by tuning the SW time. The atomic-scale electron EELS mapping profiles across the lateral edge of an SW-Cu_2O cube were also investigated (Fig. S10). It can be seen that Cu^0 in region A and Cu_2O in region B formed interconnecting interfaces in the overlapping mapping of an SW-Cu_2O cube. From the corresponding EEL spectra of Cu $L_{2,3}$-edge (Fig. 3b), the values of L_3/L_2 in regions A and B are 1.71 and 2.65, respectively, which corresponds to Cu^0 and Cu^+, confirming the existence of Cu^+ and Cu^0 interfaces on the surface of SW-Cu_2O cubes. Moreover, the surface valence state of Cu_2O before and after SW for different times was examined by X-ray photoelectron spectroscopy (XPS). The Cu 2p XPS spectra and Cu LMM (L-inner level-M-inner level-M-inner level electron transition) Auger spectra of Cu_2O before and after SW for different times are shown in Fig. S11 and Fig. 3c. In the Cu 2p XPS spectra of Cu_2O sample, the typical peaks are centered at 932.4 and

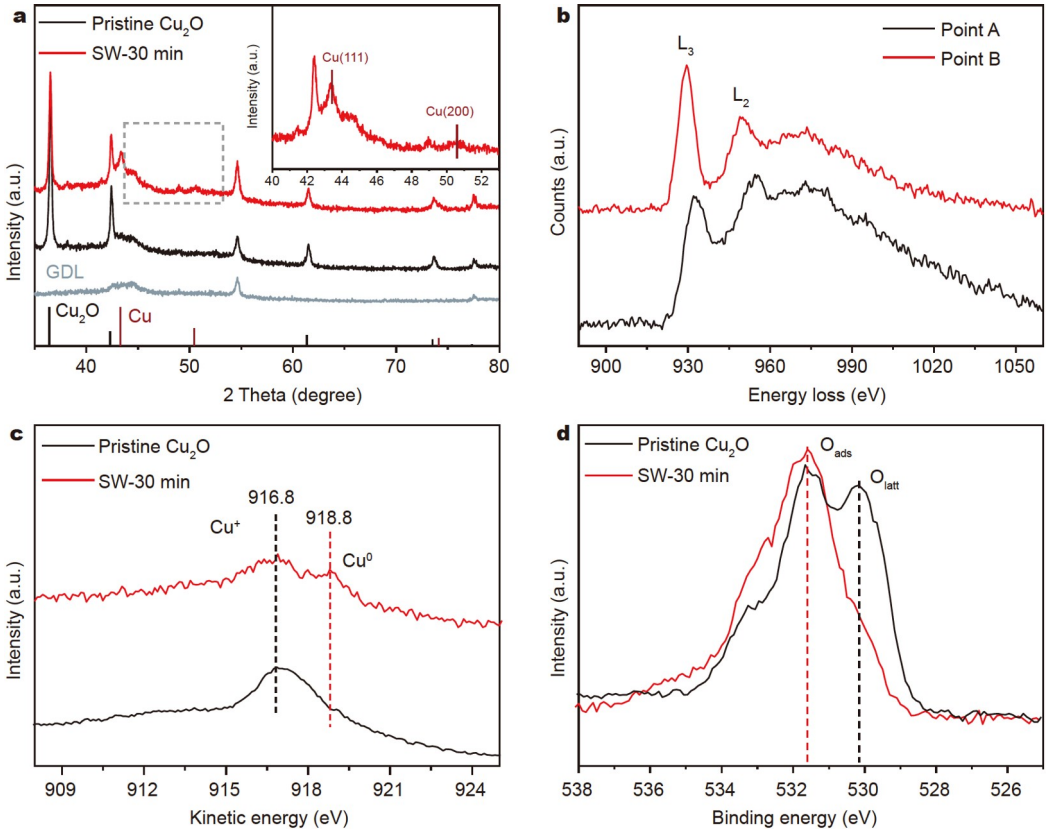

Figure 3 Structure characterization of Cu_2O before and after SW. (a) XRD patterns, (b) EEL spectra of Cu $L_{2,3}$-edge circled as point A and point B in Fig. S9, (c) Auger spectra of Cu LMM, and (d) XPS spectra of O_{ads} and O_{latt} of Cu_2O before and after 30 min SW.

952.3 eV for Cu(0)/Cu(I) species (Fig. S11a). Moreover, the kinetic energies of the main Auger peaks (Fig. S11b) are measured to be 918.8 and 916.8 eV for Cu and Cu_2O, respectively [36,37]. The presence of Cu^+ and Cu^0 species on SW-Cu_2O cubes and only Cu^+ on pristine Cu_2O cubes further demonstrate that Cu_2O cubes were partially reduced to metal Cu during the SW process, which is consistent with the conclusion from STEM-EELS and XRD analysis. In addition, the XPS spectra of O_{ads} and O_{latt} (Fig. 3d and Fig. S11c) exhibit that the O_{ads}/O_{latt} molar ratio in SW-Cu_2O is far higher than that in pristine Cu_2O, suggesting that the surface of Cu_2O was reconstructed to form Cu_2O-Cu interfaces during the SW process (Fig. 2h and Fig. S9).

ECO_2RR performance

The ECO_2RR activity of Cu_2O before and after SW treatment at different times was investigated in a CO_2-saturated 1 mol L^{-1} KCl aqueous solution using a typical H-type cell, and the catalysts were loaded onto a gas diffusion electrode. Initially, the linear-sweep voltammetry (LSV) curves (Fig. 4a), show that the fresh Cu_2O cubes and the SW-treated Cu_2O for 30 min exhibit superior current density responses and lower onset potential under the CO_2 atmosphere compared with that under the N_2 atmosphere. Moreover, the comparison of LSV curves of SW-treated Cu_2O cubes for different times clearly shows that the current density of the sample increases with the prolonging SW time till 30 min (denoted as SW-Cu_2O-30) and then decreases under CO_2 atmosphere (Fig. 4b), indicating a possibly higher activity of SW-Cu_2O cubes for ECO_2RR. Bulk electrolysis was conducted to explore the ECO_2RR performance of Cu_2O cubes after SW at different times (Fig. S12). According to the product distribution, HER is obviously suppressed on SW-Cu_2O and the best FEs for carbon products (especially C_2H_4) are obtained on the Cu_2O cubes with the SW treatment time of 30 min. However, the FE for C_2H_4 slightly decreases with further reaction time possibly due to the structure destruction of SW-Cu_2O cubes. The electrochemically active surface areas (ECSA) of Cu_2O cubes after 15–60 min of SW were investigated *via* double-layer capacitances (C_{dl}) (Fig. S13). The values of ECSA follow the trend: SW-Cu_2O-30 > SW-Cu_2O-45 > SW-Cu_2O-60 > SW-Cu_2O-15, which is in accordance with the C_2H_4 selectivity on Cu_2O cubes after different SW times. The synergistic Cu^0 and Cu^+ on Cu_2O-Cu interfaces are likely to be the key factor for the different ECSA and C_2H_4 selectivity on SW-Cu_2O. To further validate this, Cu_2O cubes were also activated by different potentials of SW and the corresponding surface valences were examined with Cu LMM Auger spectra (Fig. S14). There is no peak of Cu^0 species after pristine Cu_2O cubes activated by the reduction potential of SW below −0.2 V or oxidation potential of SW above 1.0 V, which means that Cu_2O-Cu interfaces were not formed under such conditions. As shown in Fig. S15, the C_2H_4 selectivity on Cu_2O cubes activated by a low SW reduction potential of −0.2 V or a high oxidation potential above 1.0 V is

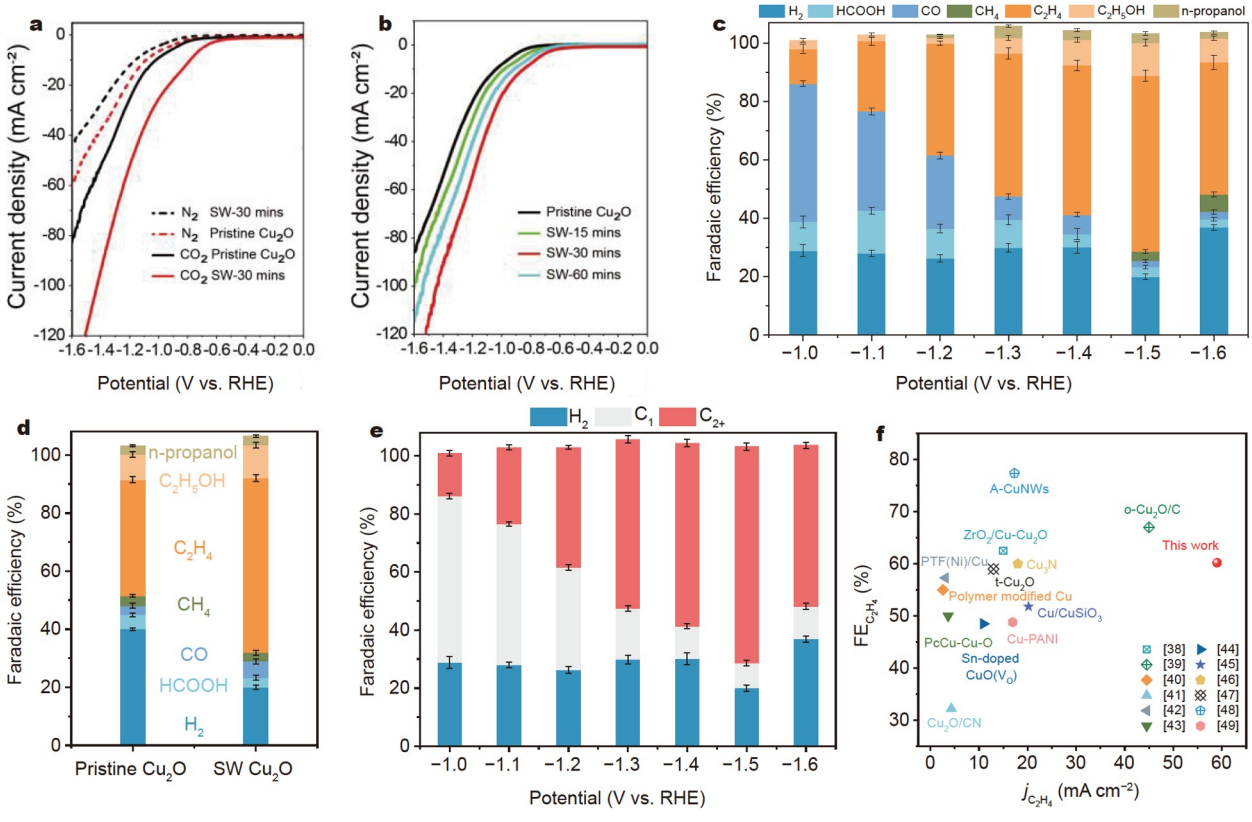

Figure 4 ECO_2RR performance of Cu_2O before and after SW. (a) LSV curves obtained at a scan rate of 1 mV s^{-1} on Cu_2O before and after 30 min SW activation. The test was performed in 1 mol L^{-1} KCl aqueous solution under CO_2 or N_2 atmosphere. (b) LSV curves of Cu_2O after different time SW for modified electrodes in a CO_2-saturated 1 mol L^{-1} KCl aqueous solution. (c) FEs of ECO_2RR products on SW-Cu_2O (SW-oxidation potential: 0.8 V; SW-reduction potential: −0.4 V; SW-time: 30 min) at the applied potentials. (d) FEs of ECO_2RR products on Cu_2O before and after SW. (e) Summary of the FEs of C_{2+}, C_1, and H_2 products for SW-Cu_2O-30 at varying applied potentials. (f) Comparison of C_2H_4 FE on Cu and Cu-based electrocatalysts reported in recent literature [38–49].

unsatisfactory. While the C_2H_4 selectivity is increased (FE for C_2H_4 reaches 60%) and the competitive HER activity is declined (FE for H_2 below 20%) when Cu_2O cubes are activated by reduction potential of −0.4 V and oxidation potential of 0.8 V for 30 min. Based on the above electrochemical tests and the surface valence analysis, the Cu_2O-Cu interfaces with suitable composition of Cu^0 and Cu^+ were built when −0.4 and 0.8 V were utilized as the reduction and oxidation potentials for 30 min.

Moreover, bulk electrolysis tests were performed on pristine Cu_2O and SW-Cu_2O-30 cubes to further prove the synergistic role of Cu^+ and Cu^0 for improving the selectivity during ECO_2RR toward C_{2+} product formation (Fig. S16). For SW-Cu_2O-30 cubes, except for the unavoidable hydrogen product, the major product is C_2H_4 when the applied potentials are above −1.2 V. Note that there are also other products such as CO, CH_4, HCOOH, C_2H_5OH, and *n*-propanol, with much lower FEs (Fig. 4c). The FE for C_2H_4 on SW-Cu_2O-30 cubes reaches 60% at −1.5 V, while it is only 39% on pristine Cu_2O cubes, as shown in Fig. 4d. Moreover, the FEs for C_{2+}, C_1 and H_2 on SW-Cu_2O-30 at applied potentials (Fig. 4e) exhibit different trends for C_1 and C_2 products; the FEs decrease as the applied potentials become more negative for the case of C_1 products and increase with the highest FE_{C2+} of 75% at −1.5 V for C_{2+} products. Compared with SW-Cu_2O-30 cubes (Fig. 4c), the FEs for H_2 are obviously increased while the FEs for C_2H_4 are decreased on the pristine Cu_2O cubes (Fig. S17). Furthermore, the total current densities and partial current densities for C_1, C_{2+} and H_2 products on SW-Cu_2O-30 electrocatalyst were evaluated at different applied potentials, as shown in Fig. S18. Specifically, the partial current density for C_2H_4 (~60 mA cm^{-2}) on SW-Cu_2O-30 cubes is about 2.3 times higher than that on pristine Cu_2O cubes (~26 mA cm^{-2}) at −1.5 V (Figs S17 and S18). The superior ECO_2RR selectivity toward C_2H_4 on SW-Cu_2O cubes further proves that the suitable synergistic Cu^+ and Cu^0 on Cu_2O-Cu interfaces play an important role in promoting C_2H_4 production, which is also in accordance with the results from DFT. The structural stability of SW-Cu_2O-30 during ECO_2RR was investigated by analyzing the structure and surface valence state of SW-Cu_2O-30 after electrolysis for 60 min, which solidly evidenced the coexistence of Cu^0 and Cu^+ in SW-Cu_2O-30 during ECO_2RR (Figs S19 and S20). A long-term stability test was further conducted over 5 h (Fig. S21). The $FE_{C_2H_4}$ shows a gradual decay from 57% to 43% and then remained unchanged. It corresponds to the disappearance of the Cu^+ and Cu^0 interfaces on SW-Cu_2O until SW-Cu_2O was completely reduced to metallic copper at negative applied potential throughout the course of the reaction (Fig. S22), which further proves the important role of the synergistic Cu^+ and Cu^0 interfaces. In addition, the ECO_2RR performance of SW-Cu_2O-30 was also compared with previously reported Cu-based electrocatalysts in an H-type cell (Fig. 4f), indicating an obvious advantage of SW-Cu_2O cubes with the competitively superior partial current density and FE for C_2H_4.

CONCLUSIONS

This study discloses the improved selectivity and activity of oxide-derived copper electrodes for C_{2+} production. DFT cacu-lations reveal that the synergistic Cu^+ and Cu^0 sites on Cu_2O-Cu interfaces endow the electrode surface with the low free energy of *COCO intermediate formation and H_2O dissociation, which are responsible for the high selectivity toward multi-carbon products, especially C_2H_4. Experimentally, pristine Cu_2O cubes were chosen as the model, and further activated *via* suitable SW to obtain SW-Cu_2O/Cu cubes with synergistic Cu^0 and Cu^+ on Cu_2O-Cu interfaces. The FEs for C_2H_4 (~60%) and C_{2+} products (~75%) on SW-Cu_2O cubes are about 1.5 times higher than that on pristine Cu_2O cubes. Moreover, the as-prepared SW-Cu_2O/Cu-30 cubes also exhibit a superior partial current density for C_2H_4 (~60 mA cm^{-2}) during ECO_2RR in an H-type cell, which is about 2.3 times higher than that of pristine Cu_2O cubes. Therefore, creating effective interfaces with synergistic Cu^0 and Cu^+ species offers insight into improving the selectivity of a specific valuable multi-carbon product and promotes practical CO_2 conversion technology.

Received 13 September 2022; accepted 30 November 2022; published online 17 February 2023

1 Lee MY, Park KT, Lee W, *et al.* Current achievements and the future direction of electrochemical CO_2 reduction: A short review. Crit Rev Environ Sci Tech, 2019, 50: 769–815
2 De Luna P, Hahn C, Higgins D, *et al.* What would it take for renewably powered electrosynthesis to displace petrochemical processes? Science, 2019, 364: aav3506
3 Peter SC. Reduction of CO_2 to chemicals and fuels: A solution to global warming and energy crisis. ACS Energy Lett, 2018, 3: 1557–1561
4 Qiao J, Liu Y, Hong F, *et al.* A review of catalysts for the electroreduction of carbon dioxide to produce low-carbon fuels. Chem Soc Rev, 2014, 43: 631–675
5 Li X, Wu X, Lv X, *et al.* Recent advances in metal-based electrocatalysts with hetero-interfaces for CO_2 reduction reaction. Chem Catal, 2021, 2: 262–291
6 Wang D, Chang K, Zhang Y, *et al.* Unravelling the electrocatalytic activity of bismuth nanosheets towards carbon dioxide reduction: Edge plane *versus* basal plane. Appl Catal B-Environ, 2021, 299: 120693
7 Wang D, Liu C, Zhang Y, *et al.* CO_2 electroreduction to formate at a partial current density up to 590 mA mg^{-1} *via* micrometer-scale lateral structuring of bismuth nanosheets. Small, 2021, 17: 2100602
8 Liang S, Huang L, Gao Y, *et al.* Electrochemical reduction of CO_2 to CO over transition metal/N-doped carbon catalysts: The active sites and reaction mechanism. Adv Sci, 2021, 8: 2102886
9 Wang X, Feng S, Lu W, *et al.* A new strategy for accelerating dynamic proton transfer of electrochemical CO_2 reduction at high current densities. Adv Funct Mater, 2021, 31: 2104243
10 Wakerley D, Lamaison S, Ozanam F, *et al.* Bio-inspired hydrophobicity promotes CO_2 reduction on a Cu surface. Nat Mater, 2019, 18: 1222–1227
11 Nitopi S, Bertheussen E, Scott SB, *et al.* Progress and perspectives of electrochemical CO_2 reduction on copper in aqueous electrolyte. Chem Rev, 2019, 119: 7610–7672
12 Popović S, Smiljanić M, Jovanovič P, *et al.* Stability and degradation mechanisms of copper-based catalysts for electrochemical CO_2 reduction. Angew Chem Int Ed, 2020, 59: 14736–14746
13 Gao D, Arán-Ais RM, Jeon HS, *et al.* Rational catalyst and electrolyte design for CO_2 electroreduction towards multicarbon products. Nat Catal, 2019, 2: 198–210
14 Lei Q, Zhu H, Song K, *et al.* Investigating the origin of enhanced C_{2+} selectivity in oxide-/hydroxide-derived copper electrodes during CO_2 electroreduction. J Am Chem Soc, 2020, 142: 4213–4222
15 Kuhl KP, Cave ER, Abram DN, *et al.* New insights into the electrochemical reduction of carbon dioxide on metallic copper surfaces. Energy Environ Sci, 2012, 5: 7050–7059
16 Zheng Y, Vasileff A, Zhou X, *et al.* Understanding the roadmap for electrochemical reduction of CO_2 to multi-carbon oxygenates and hydrocarbons on copper-based catalysts. J Am Chem Soc, 2019, 141: 7646–7659

17 Velasco-Vélez JJ, Jones T, Gao D, *et al.* The role of the copper oxidation state in the electrocatalytic reduction of CO_2 into valuable hydrocarbons. ACS Sustain Chem Eng, 2019, 7: 1485–1492
18 Mistry H, Varela AS, Bonifacio CS, *et al.* Highly selective plasma-activated copper catalysts for carbon dioxide reduction to ethylene. Nat Commun, 2016, 7: 12123
19 Wang J, Tan HY, Zhu Y, *et al.* Linking the dynamic chemical state of catalysts with the product profile of electrocatalytic CO_2 reduction. Angew Chem Int Ed, 2021, 60: 17254–17267
20 Kim D, Lee S, Ocon JD, *et al.* Insights into an autonomously formed oxygen-evacuated Cu_2O electrode for the selective production of C_2H_4 from CO_2. Phys Chem Chem Phys, 2014, 17: 824–830
21 Yang PP, Zhang XL, Gao FY, *et al.* Protecting copper oxidation state *via* intermediate confinement for selective CO_2 electroreduction to C_{2+} fuels. J Am Chem Soc, 2020, 142: 6400–6408
22 Arán-Ais RM, Scholten F, Kunze S, *et al.* The role of *in situ* generated morphological motifs and Cu(I) species in C_{2+} product selectivity during CO_2 pulsed electroreduction. Nat Energy, 2020, 5: 317–325
23 Tang HF, Huang ZY, Xiao M. Effects of particle size and temperature on surface thermodynamic functions of cubic nano-Cu_2O. Acta Physico-Chim Sin, 2016, 32: 2678–2684
24 Kresse G, Furthmüller J. Efficiency of *ab-initio* total energy calculations for metals and semiconductors using a plane-wave basis set. Comput Mater Sci, 1996, 6: 15–50
25 Kresse G, Furthmüller J. Efficient iterative schemes for *ab initio* total-energy calculations using a plane-wave basis set. Phys Rev B, 1996, 54: 11169–11186
26 Kresse G, Joubert D. From ultrasoft pseudopotentials to the projector augmented-wave method. Phys Rev B, 1999, 59: 1758–1775
27 Perdew JP, Burke K, Ernzerhof M. Generalized gradient approximation made simple. Phys Rev Lett, 1998, 77: 3865–3868
28 Gao Y, Chen Z, Zhu Y, *et al.* New insights into the generation of singlet oxygen in the metal-free peroxymonosulfate activation process: Important role of electron-deficient carbon atoms. Environ Sci Technol, 2020, 54: 1232–1241
29 De Luna P, Quintero-Bermudez R, Dinh CT, *et al.* Catalyst electroredeposition controls morphology and oxidation state for selective carbon dioxide reduction. Nat Catal, 2018, 1: 103–110
30 Todorova TK, Schreiber MW, Fontecave M. Mechanistic understanding of CO_2 reduction reaction (CO_2RR) toward multicarbon products by heterogeneous copper-based catalysts. ACS Catal, 2019, 10: 1754–1768
31 Kortlever R, Shen J, Schouten KJP, *et al.* Catalysts and reaction pathways for the electrochemical reduction of carbon dioxide. J Phys Chem Lett, 2015, 6: 4073–4082
32 Mandal SC, Rawat KS, Garg P, *et al.* Hexagonal Cu(111) monolayers for selective CO_2 hydrogenation to CH_3OH: Insights from density functional theory. ACS Appl Nano Mater, 2019, 2: 7686–7695
33 Guo X, Liu S, Huang S. Single Ru atom supported on defective graphene for water splitting: DFT and microkinetic investigation. Int J Hydrogen Energy, 2018, 43: 4880–4892
34 Wu T, López N, Vegge T, *et al.* Facet-dependent electrocatalytic water splitting reaction on CeO_2: A DFT + *U* study. J Catal, 2020, 388: 1–10
35 Li P, Xie Q, Zheng L, *et al.* Topotactic reduction of layered double hydroxides for atomically thick two-dimensional non-noble-metal alloy. Nano Res, 2017, 10: 2988–2997
36 Yang F, Deng PL, Wang Q, *et al.* Metal-organic framework-derived cupric oxide polycrystalline nanowires for selective carbon dioxide electroreduction to C2 valuables. J Mater Chem A, 2020, 8: 12418–12423
37 Martin L, Martinez H, Poinot D, *et al.* Comprehensive X-ray photoelectron spectroscopy study of the conversion reaction mechanism of CuO in lithiated thin film electrodes. J Phys Chem C, 2013, 117: 4421–4430
38 Guo PP, He ZH, Yang SY, *et al.* Electrocatalytic CO_2 reduction to ethylene over ZrO_2/Cu-Cu_2O catalysts in aqueous electrolytes. Green Chem, 2022, 24: 1527–1533
39 Gao Y, Yu S, Zhou P, *et al.* Promoting electrocatalytic reduction of CO_2 to C_2H_4 production by inhibiting C_2H_5OH desorption from Cu_2O/C composite. Small, 2022, 18: 2105212
40 Wang J, Cheng T, Fenwick AQ, *et al.* Selective CO_2 electrochemical reduction enabled by a tricomponent copolymer modifier on a copper surface. J Am Chem Soc, 2021, 143: 2857–2865
41 Zhang J, Guo Y, Shang B, *et al.* Unveiling the synergistic effect between graphitic carbon nitride and Cu_2O toward CO_2 electroreduction to C_2H_4. ChemSusChem, 2021, 14: 929–937
42 Meng DL, Zhang MD, Si DH, *et al.* Highly selective tandem electroreduction of CO_2 to ethylene over atomically isolated nickel-nitrogen site/copper nanoparticle catalysts. Angew Chem Int Ed, 2021, 60: 25485–25492
43 Qiu XF, Zhu HL, Huang JR, *et al.* Highly selective CO_2 electroreduction to C_2H_4 using a metal-organic framework with dual active sites. J Am Chem Soc, 2021, 143: 7242–7246
44 Jiang Y, Choi C, Hong S, *et al.* Enhanced electrochemical CO_2 reduction to ethylene over CuO by synergistically tuning oxygen vacancies and metal doping. Cell Rep Phys Sci, 2021, 2: 100356
45 Yuan X, Chen S, Cheng D, *et al.* Controllable Cu^0-Cu^+ sites for electrocatalytic reduction of carbon dioxide. Angew Chem Int Ed, 2021, 60: 15344–15347
46 Yin Z, Yu C, Zhao Z, *et al.* Cu_3N nanocubes for selective electrochemical reduction of CO_2 to ethylene. Nano Lett, 2019, 19: 8658–8663
47 Gao Y, Wu Q, Liang X, *et al.* Cu_2O nanoparticles with both {100} and {111} facets for enhancing the selectivity and activity of CO_2 electroreduction to ethylene. Adv Sci, 2020, 7: 1902820
48 Choi C, Kwon S, Cheng T, *et al.* Highly active and stable stepped Cu surface for enhanced electrochemical CO_2 reduction to C_2H_4. Nat Catal, 2020, 3: 804–812
49 Wei X, Yin Z, Lyu K, *et al.* Highly selective reduction of CO_2 to C_{2+} hydrocarbons at copper/polyaniline interfaces. ACS Catal, 2020, 10: 4103–4111

Acknowledgements This work was supported by the National Key Research and Development Project (2018YFB1502401 and 2018YFA0702002), the Program for Changjiang Scholars and Innovation Research Team in the University (IRT1205), the Fundamental Research Funds for the Central Universities, and the long-term subsidy mechanism from the Ministry of Finance and the Ministry of Education of China. We thank Lu Bai for her help in electron microscopy characterization.

Author contributions Wang S carried out the experiments and analyzed the data. Wang D participated in the data analysis, and writing and editing of the manuscript. Tian B plotted figures and assisted in the experiments and data analysis. Gao X carried out the DFT calculations. Han L, Zhong Y, Song S and Wang Z assisted to carry out electrochemical experiments. Li Y directed the DFT calculations. Gui J took part in the format editing of the manuscript. Zhang Y supervized the project and participated in editing and review of the manuscript. Kuang Y and Sun X provided resources, and directed the research.

Conflict of interest The authors declare that they have no conflict of interest.

Supplementary information Experimental details and supporting data are available in the online version of the paper.

Ying Zhang received her PhD degree in 2019 from Monash University, Australia, under the supervision of Prof. Jie Zhang and Prof. Alan. M. Bond. Currently, she is an associate professor at Jiangnan University, China. Her research focuses on electrochemical reduction of CO_2 including developing efficient catalysts and fundamental study of mechanisms.

Yun Kuang obtained his PhD degree in 2015 and joined the College of Chemistry, Beijing University of Chemical Technology in the same year. His recent research focuses on the design of material interface for active and stable electrocatalysis in energy and environment-related processes.

Cu_2O-Cu界面上的Cu^+和Cu^0协同促进电催化CO_2还原高效和高选择性地生成C_{2+}产物

王胜楠[1,2†], 王丹[1†], 田本强[2†], 高响响[2†], 韩璐[2], 钟洋[3], 宋舒畅[2], 王智立[2], 李亚平[2], 归家宁[1], Marshet G. Sendeku[4], 张颖[1*], 邝允[2*], 孙晓明[2]

摘要 电催化CO_2还原技术有望同时缓解化石燃料濒临枯竭及大气中CO_2浓度不断攀升等问题. 然而, 对于高附加值的电催化CO_2还原多碳产物的选择性提升, 仍然面临巨大挑战. 密度泛函理论(DFT)计算表明, Cu_2O-Cu界面上Cu^+和Cu^0的协同耦合效应使其表面上*COCO中间体的生成能降低, 同时H_2O的解离自由能也降低, 从而有利于电催化CO_2还原高选择性生成多碳产物特别是C_2H_4. 受DFT计算结果的启发, 本文设计了一种氧化物衍生铜电极的活化策略, 构建Cu_2O-Cu界面, 以Cu^+和Cu^0协同促进电催化CO_2还原高效高选择性生成C_{2+}产物. 其中, Cu_2O立方体被用作初始催化剂, 经方波电位处理后, 在Cu_2O-Cu界面上形成了具有Cu^+和Cu^0协同作用的SW-Cu_2O/Cu立方体. 在H型电解池中, SW-Cu_2O/Cu电催化CO_2还原生成C_2H_4和C_{2+}产物的法拉第效率分别为60%和75%, 约为前驱体Cu_2O立方体的1.5倍, 证明Cu^0和Cu^+在Cu_2O-Cu界面上的协同作用的确可提高电催化CO_2还原过程中特定高附加值多碳产物的选择性.